

Numerical Investigation of the Effects of Chemical Species and Chemical Kinetic Mechanisms on Laminar Premixed Flame-Acoustic Wave Interactions

E. Salimi Babokani, M. Davazdah Emami[†] and A. R. Pishevar

Department of Mechanical Engineering, Isfahan University of Technology, Isfahan 8415683111, Iran

[†]Corresponding Author Email: mohsen@cc.iut.ac.ir

(Received July 11, 2022; accepted November 14, 2022)

ABSTRACT

Numerical simulation of interactions between acoustic waves and flames is of utmost importance in thermo-acoustic instability research. In this study, interactions between a one-dimensional Methane-Air laminar premixed flame and acoustic waves with a frequency of 50 to 50000 Hz are simulated by simultaneously solving the equations for energy conservation, chemical species transport, state and continuity in one-dimensional space. By assuming that the flame thickness is smaller than the acoustic wavelength, the spatial pressure fluctuations can be neglected and the flame experiences only a time-varying acoustic pressure. The GRI mechanisms, as well as their reduced mechanisms, are considered to obtain results for steady flames without acoustic waves, and the interaction of unsteady flames with acoustic waves. Results show that the total heat-release-rate fluctuations for the flame is affected by increasing the frequency of the acoustic wave. An increase in frequency first increases the total heat released, and then decreases it. The obtained results are in good agreement with those of other researchers. Furthermore, at the presence of acoustic waves, various chemical species can affect the total heat-release-rate fluctuations. With Rayleigh's instability criterion, it can be shown that H₂O, CO₂ and O₂ are the main species to the fluctuations of the total heat release rate and lead to flame instability. Results show that heat-release-rate of H₂O specie is the most important on the total heat-release-rate. Therefore, for the flame-acoustic waves interaction problem, the best mechanism is the one that could predict the concentration of H₂O more precisely.

Keywords: Flame-acoustic interaction; Rayleigh instability; Numerical simulation; Acoustic waves; Multistep mechanisms.

1. INTRODUCTION

One of the most influential factors in combustion in some flames is the interaction between acoustic waves and flame. Studying the effects of acoustic waves on the flame is vital for various reasons. The generated noise during combustion, and its interaction with the flame, may result in unstable combustion. This phenomenon is most evident in equipment outfitted with a combustion chamber, such as gas turbines and ramjets. Combustion instability can lead to flame extinguishment, or damage to the combustion chamber. However, there are also some cases, where the generation of acoustic waves can improve flame stability or soot reduction in the combustion chamber (Demare and Baillot 2004). Other applications of acoustic waves and flame interaction are enhancement to fuel and air mixture, increase in combustion efficiency, and reduction in NO_x pollutions (Chao *et al.* 1996; Oh *et al.* 2009; Fujisawa *et al.* 2019). Given these features,

it is crucial to study combustion instability to control the combustion process.

Combustion instability generally appears as high amplitude pressure fluctuations due to the resonance at the natural frequency of combustion chamber (Lieuwen and Yang 2005). Thermo-acoustic instability is the result of a combined heat-release-rate fluctuations from the flame and acoustic waves. By studying the interactions of flame and acoustic waves, in 1878, Rayleigh presented a criterion for combustion instability as follows (Rayleigh 1945):

$$\int_0^T \int_0^V p'(x,t) \cdot q'(x,t) dv dt > \int_0^T \int_0^V \Phi(x,t) dv dt \quad (1)$$

Where p' and q' are pressure and heat-release-rate fluctuations, respectively, Φ is the dissipation of energy in the system, v denotes volume, and t is a long enough time interval. This equation illustrates that when added energy to the system (left-hand-side of the inequality, or gains) is more than the

dissipation of energy (right-hand-side of the inequality, or losses), instability increases.

In most combustion systems, the dissipation of energy is minimal, and the right-hand side of the inequality diminishes. Thus, Rayleigh's combustion instability criterion may be considered as follows:

$$\int_0^V \int_0^T p'(x,t) \cdot q'(x,t) dv dt > 0 \quad (2)$$

When the phase difference between pressure fluctuations and heat release fluctuations is below 90 degrees, the left-hand side of the equation is larger than zero, and the system destabilizes. If the difference is anything between 90 and 180 degrees, the left-hand side of the equation is negative, resulting in the stabilization of the system (Lieuwen and Yang 2005).

(Clavin and Pelce 1989) assumed the effects of pressure fluctuations on a flat premixed flame to be one-dimensional and solved the equations for mass conservation, momentum, and energy. They also studied the equation for chemical species conservation, using a single-step Arrhenius reaction for the chemical kinetics. They collided a single acoustic wave, with a short amplitude of p' and medium frequencies of ω to a laminar flame of thickness δ_f at a velocity of S_f . In a similar study, (Mcintosh 1991, 1993, 1999) calculated the fluctuations for mass flux and heat-release-rate. Moreover, in another study by (Jiménez *et al.* 2012), they used a two-step reaction for chemical kinetics. Numerical predictions from their studies show similarities to the single-step model results in lower frequencies. However, at higher frequencies, results differed from the single-step model.

To verify the one-dimensional thermo-acoustic theory, (Wangher *et al.* 2008) studied the effect of an acoustic wave on premixed one-dimensional flames of Methane and Propane. They considered the acoustic wave's frequency in the range of 90 to 1000 Hz. By comparing the chemical luminescence results for Hydroxyl (OH*) and Methylidyne (CH*) radicals with those from theoretical equations, it was found that these results show similarities to the heat-release-rate fluctuations, and differ from the that of fuel consumption theory. With an increase in frequency, the amplitude for the heat-release-rate fluctuations nearly remains constant. Comparison of experimental data and theoretical results show similarities based on order but differ numerically. They presented two reasons for this numerical difference. The primary reason was the inaccuracy of the single-step mechanism for analyzing chemical kinetics. Also, chemical luminescence of OH* was determined to be unsuitable for calculating heat-release-rate fluctuations.

(Schmidt and Jiménez 2010) numerically studied the interaction of acoustic waves with a premixed Methane flame based on the research of (Wangher *et al.* 2008). They presented two numerical solutions based on the assumption of compressible and incompressible flows. By assuming the Mach number to be small and considering the equations for

energy and species conservation (Klein 1995), they calculated the incompressible solution for the one-dimensional problem. Using the DNS method (Baum *et al.* 1995), they were also able to calculate the compressible solution for the same problem. To investigate the effects of chemical kinetics, they used the advanced GRI-3.0 model (Smith *et al.* n.d.) (53 species, 325 reactions), Peter's multi-step model (Peters 1996) (16 species), and the Arrhenius single-step model (Fernandez-Tarrazo *et al.* 2006). Simulation results showed the compressible and incompressible models have little differences. This conclusion could be a result of excluding the pressure gradient term from the equations. Comparisons showed the results were in good agreement with data obtained by the experimental model (Wangher *et al.* 2008), rather than those based on the theoretical model (Clavin and Pelce 1989; Mcintosh 1991). By studying the models for chemical kinetics, it was shown that the results for the GRI-3.0 and Peter's models were in accordance, while they considerably differed from the Arrhenius single-step model. Finally, they concluded, that the single-step model was unable to make correct predictions regarding the interactions between the acoustic waves and flame.

(Jiménez *et al.* 2012) following their previous research, studied and calculated the interaction between an acoustic wave and a flat premixed flame. The GRI-3.0 and San Diego (Saxena and Williams 2006) (21 reactions) models were used to simulate combustion for Methane and Hydrogen, respectively. Simulation results were compared with data acquired from single-step (Clavin and Pelce 1989), and two-step (Clavin and Searby 2008) theoretical model and experimental data. Results for the two-step theoretical model have better agreement with the experimental and numerical data. Eventually, they suggested multi-step kinetic models to study the interactions between the acoustic waves and flame.

(Beardsell and Blanquart 2019) calculated the interactions of acoustic waves with a premixed Methane-Air flame and compared their results with (Wangher *et al.* 2008) and (Jiménez *et al.* 2012) results. In addition to using Methane as fuel for the laminar premixed flame, they used n-Heptane and n-Dodecane, and studied the interactions of acoustic waves on their flames. Based on Rayleigh's definition of instability, they assessed the corresponding frequency with maximum fluctuations of heat-release-rate and zero-phase-difference, as the unstable frequency. (Beardsell and Blanquart 2021) numerically simulated the laminar flame and acoustic waves interaction problem for hydrogen and n-heptane fuels.

Performing two and three-dimensional simulation of the interactions between acoustic waves and flames is costly for combustion models based on transport equation (e.g. Eddy Dissipation Concept Model). Based on this fact, researchers prefer to use single or two-step mechanisms to simulate chemical kinetics (Han and Morgans 2015; Han *et al.* 2016; Hajjaligol and Mazaheri 2017; Lee and Cant 2017; Massey *et al.* 2018). Therefore, assessing the reduced states of

chemical mechanisms is essential in determining an accurate and cost-efficient mechanism.

(Shalaby *et al.* 2009) studied the interactions of acoustic waves with a turbulent premixed flame, using the DNS simulation method. Based on Rayleigh's instability criterion, CO₂, H₂O, and H have positive values, meaning they increase instability, while O, OH, and CO have negative values and contribute to the dissolution of the acoustic wave. HCO, CH₂O, HO₂, and H₂O₂ radicals have near-zero values, meaning they have little to no effect on the interaction process. Neutral species such as Argon (Ar) and Nitrogen (N₂), have been found to have near-zero values as well. Findings from these researches show that the two models used for studying chemical kinetics produce different results, especially for species such as CO₂, H₂O, H, and OH.

(Laverdant and Thevenin 2003), studied the effects of Gaussian sound waves on a turbulent non-premixed Hydrogen flame, using the DNS method. Rayleigh's instability values were in agreement with the heat-release-rate fluctuations. H₂O₂ and HO₂ have near-zero values, while H₂, O₂, and especially H₂O contribute to the increase of instability. H* is an essential factor in the dissipation of the acoustic wave.

It is prominent to consider the heat-release-rate fluctuations of chemical species to obtain the effect of each chemical species on system instability.

The goal of this research is:

- 1- Assessing the reduced states of chemical mechanisms is essential in determining an accurate and cost-efficient mechanism.
- 2- Assessing the contribution of each species on destabilizing the reaction. Moreover, by determining the impact of each species, we can justify the difference results from different chemical kinetic mechanisms.

2. METHODOLOGY

2.1 The Governing Equations

Zero-Mach-number equations (Schmidt and Jiménez 2010) for simulating the interaction of the acoustic wave and laminar flat flame are as follows:

Species Transport Equation:

$$\rho \frac{\partial Y_s}{\partial t} + \rho u \frac{\partial Y_s}{\partial x} = -\frac{\partial j_s}{\partial x} + M_s \dot{\omega}_s \quad (3)$$

Energy Equation:

$$\rho c_p \frac{\partial T}{\partial t} + \rho u c_p \frac{\partial T}{\partial x} = \frac{dp}{dt} - \frac{\partial q}{\partial x} - \sum_s j_s \frac{\partial h_s}{\partial x} - \sum_s h_s M_s \dot{\omega}_s \quad (4)$$

Continuity Equation:

$$\frac{\partial \rho}{\partial t} + \frac{\partial}{\partial x}(\rho u) = 0 \quad (5)$$

In the above equations, subscript (_s) denotes species *s*, ρ is the density of the mixture, Y_s is the mass fraction of species *s*, u represents velocity, $j_s = -\rho D_{sm} \partial Y_s / \partial x$ is the diffusion flux of species *s*, D_{sm} is the mass diffusion coefficient of species *s*, M_s denotes the molecular weight of species *s*, $\dot{\omega}_s$ is the chemical source term of species *s*, c_p is the specific heat of the mixture at constant pressure, p is the pressure, $q = -k \partial T / \partial x$ is the Fourier's thermal flux, k is the conductive heat transfer coefficient, and h_s is the enthalpy of species *s*.

State equation for a mixture of ideal gases is as follows:

$$p = \rho T \sum_s Y_s R_s \quad (6)$$

where R_s is the gas constant for species *s*.

With spatial and temporal differentiation of the state equation, and applying the equations for species transport and energy in the continuity equation, while $dp/dx = 0$, a definitive equation for velocity is obtained:

$$\frac{\partial u}{\partial x} = C + D + CH \quad (7)$$

In the above equation, term *C* is the compression term resulted from combining state and continuity equations, *D* is the diffusion term, and *CH* is the chemical reaction term.

$$C = -\frac{1}{\gamma p} \frac{dp}{dt} \quad (8)$$

$$D = -\frac{1}{\rho c_p T} \left\{ \frac{\partial q}{\partial x} + \sum_s j_s \frac{\partial h_s}{\partial x} \right\} - \frac{1}{\rho} \sum_s \left\{ \frac{M}{M_s} \frac{\partial j_s}{\partial x} \right\} \quad (9)$$

$$CH = \frac{1}{\rho} \sum_s \left\{ \frac{M}{M_s} - \frac{h_s}{c_p T} \right\} M_s \dot{\omega}_s \quad (10)$$

$M = 1 / \sum_{s=1}^S Y_s / M_s$ is the molecular weight of the mixture, and $\gamma = c_p / c_v$ is the ratio of specific heats.

By assuming that the acoustic wave-length is relatively larger than the flame's thickness, one may disregard the spatial pressure fluctuations, and the temporal pressure fluctuations can be calculated by the following equation:

$$\frac{dp}{dt} = A \omega \cos(\omega t) \quad (11)$$

Table 1 Chemical reaction mechanism

Mechanism	No. of Species	No. of Reactions	Method of Reduction	Ref.
GRI-1.2	32	177	-	(Frenklach <i>et al.</i> 1995)
Drm22	24	104	detailed reduction	(Kazakov and Frenklach n.d. b)
Drm19	21	84	detailed reduction	(Kazakov and Frenklach n.d. a)
10step	14	10	steady-state analysis	(Chang and Chen n.d.)
6step	10	6	steady-state analysis	(Chang and Chen n.d.)
GRI-2.11	49	279	-	(Bowman <i>et al.</i> n.d.)
16step(ARM2)	19	16	steady-state analysis	(Tang 2003)
12step	16	12	steady-state analysis	(Chen n.d.)
GRI-3.0	53	325	-	(Smith <i>et al.</i> n.d.)
15step	19	15	steady-state analysis	(Sung <i>et al.</i> 2001)
13step	17	13	steady-state analysis	(Chen n.d.)

where A is the amplitude of pressure fluctuations, and f is the frequency of the acoustic wave, $\omega = 2\pi f$. In the above equations, thermodynamic and transfer parameters can be calculated by the following equations:

$$c_{ps} = \frac{R}{M_s} \left[a_{1s} + a_{2s}T_s + a_{3s}T_s^2 + a_{4s}T_s^3 + a_{5s}T_s^4 \right] \quad (12)$$

$$c_p = \sum_{s=1}^S c_{ps} Y_s \quad (13)$$

$$h_s = \frac{RT}{M_s} \left[a_{1s} + \frac{a_{2s}}{2} T_s + \frac{a_{3s}}{3} T_s^2 + \frac{a_{4s}}{4} T_s^3 + \frac{a_{5s}}{5} T_s^4 + \frac{a_{6s}}{T_s} \right] \quad (14)$$

$$k = \frac{1}{2} \left(\sum_{s=1}^S X_s k_s + \frac{1}{\sum_{s=1}^S X_s / k_s} \right) \quad (15)$$

where c_{ps} is the constant pressure specific heat of species s , X_s is the mole fraction of species s , and a are constants of the equation. Chemical reaction rates for the I reactions containing species s are calculated by the following

equation:

$$\dot{\omega}_s = \sum_{i=1}^I (v''_{si} - v'_{si}) \left[k_{fi} \prod_{s=1}^S [X_s]^{v'_{si}} - k_{ri} \prod_{s=1}^S [X_s]^{v''_{si}} \right] \quad (16)$$

where v'_{si} and v''_{si} are stoichiometric coefficients for the forward and reverse reactions, respectively. $[X_s]$ is the molar concentration for species s , k_{fi} and k_{ri} are the forward and reverse rate constants, which can be calculated by the following equations:

$$k_{fi} = A_i T^{\beta_i} \exp\left(\frac{-E_i}{R_c T}\right) \quad (17)$$

$$k_{ri} = \frac{k_{fi}}{K_{ci}} \quad (18)$$

Where A_i is the pre-exponential factor in the rate constant of the i^{th} reaction, β_i is the temperature exponent in the rate constant of the i^{th} reaction, E_i is the activation energy in the rate constant of the i^{th} reaction, R_c is the universal gas constant in [cal / (mole K)] and K_{ci} is the equilibrium constant in concentration units for the i^{th} reaction.

2.2 Chemical Kinetic Mechanisms

The chemical reactions in the equations are obtained by using the reduced states of GRI-1.2, GRI-2.11, and GRI-3.0 mechanisms. Table 1 provides the number of chemical species and reactions for these chemical mechanisms.

2.3 Numerical Simulation

At each time step, pressure can be calculated explicitly using Eq. (6). Energy and species transport equations are discretized by an implicit second-order spatial and temporal finite difference scheme to solve for mass fractions of species and temperature at any point. Density is determined by the state equation and velocity is explicitly achieved from Eq. (7). k , c_p , h_s , D_{sm} and $\dot{\omega}_s$ can be calculated by CHEMKIN2 (Kee *et al.* 1989) having state variables at any point.

2.4 Initial and Boundary Conditions

A schematic of the solution domain is presented in Fig. 1. The length of the computational domain and the flame's thickness is relatively smaller than the acoustic wavelength. Thus, it is possible to assume constant pressure along the length of the domain. The

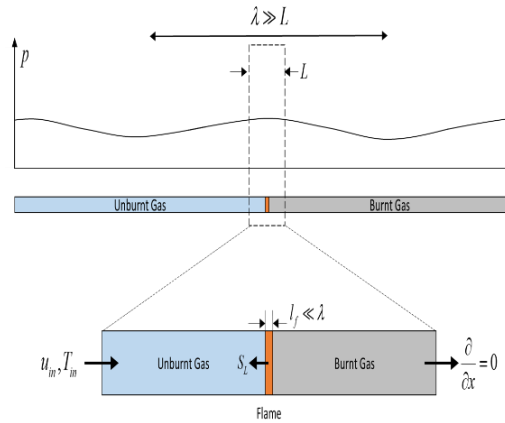


Fig. 1. Schematics of the domain.

unburnt mixture enters from the left boundary with u_{in} and T_{in} as inlet velocity and temperature, respectively. The velocity and temperature for the inlet boundary can be calculated using the following equations:

$$u_{in} = \bar{u}_{in} + u'_{in} \quad (19)$$

$$T_{in} = \bar{T}_{in} + T'_{in} \quad (20)$$

Average values of 13cm/s and 300K were assumed for velocity and temperature, respectively. Velocity and temperature fluctuation values can be calculated, using the following equations (Shreekrishna and Lieuwen 2009):

$$\frac{T'_{in}}{\bar{T}_{in}} = \left(1 + \frac{P'}{\bar{P}}\right)^{\frac{\gamma-1}{\gamma}} - 1 \quad (21)$$

$$\frac{u'_{in}}{\bar{u}_{in}} = \gamma M_0 \frac{P'}{\bar{P}} \quad (22)$$

However, these values have little effects on the solution. The Mach-number value for Eq. (22) is very small and this equation has been ignored in the previous researches (Schmidt and Jiménez 2010; Beardsell and Blanquart 2019).

At the inlet boundary, mass flux fractions were assumed instead of species mass fractions. Mass flux fractions can be calculated using the following equations:

$$\varepsilon_s = Y_s + \frac{D_{sm}}{u} \frac{\partial Y_s}{\partial x} \quad (23)$$

The gradients of temperature and species mass fractions are set to zero at the outlet boundary. The steady-state solution of equations was used as the initial condition for studying the interaction between the flame and acoustic waves. The steady solution is obtained by considering a zero value for the frequency in Eq. (11), and the compression term in Eq. (8) ($C=0$).

2.5 Non-dimensional Parameters

The non-dimensional parameters are introduced in

this section to enable us to make a better comparison between the acquired results with other experimental and numerical data. The flame transient time scale (Jiménez *et al.* 2012), is defined as:

$$\tau_t = \frac{a}{S_L^2} \quad (24)$$

where a is the thermal diffusivity and S_L is the laminar flame speed. The flame thickness length scale l_f is defined as (Beardsell and Blanquart 2019):

$$l_f = \frac{T_b - T_u}{\max\left(\frac{\partial T}{\partial x}\right)} \quad (25)$$

where T_b and T_u are the temperatures for burnt and unburnt fuel, respectively. The heat-release-rate for species s and total heat-release-rate for N_s amount of chemical species are as follows:

$$Q_s = -M_s \dot{\omega}_s h_s \quad (26)$$

$$Q_{tot} = \sum_{s=1}^{N_s} Q_s \quad (27)$$

$$= - \sum_{s=1}^{N_s} M_s \dot{\omega}_s h_s$$

To study the heat-release-rate fluctuations in time, it is necessary to use the integral of heat-release-rate on the whole domain. Therefore, the total heat-release-rate and the species heat-release-rate s are defined:

$$\Phi_s = \int_0^L Q_s dx \quad (28)$$

$$\Phi_{tot} = \int_0^L Q_{tot} dx \quad (29)$$

Now, if the integral variations of the heat-release-rate in time are divided into averaged and fluctuating parts:

$$\Phi_s = \bar{\Phi}_s + \Phi'_s \quad (30)$$

$$\Phi_{tot} = \bar{\Phi}_{tot} + \Phi'_{tot} \quad (31)$$

Then the ratio of the total heat-release-rate fluctuations to the pressure fluctuations can be defined as:

$$G = \frac{\Phi'_{tot,max} / \bar{\Phi}_{tot}}{p'_{max} / \rho c^2} \quad (32)$$

where $\Phi'_{tot,max}$ and p'_{max} are the amplitude for Φ_{tot} and p , respectively. The phase difference between the total heat-release-rate and pressure, and the species heat-release-rate s and pressure can also be calculated as follows:

$$\Theta = 2\pi f (t_{p_{\max}} - t_{\Phi_{tot,\max}}) \quad (33)$$

$$\Theta_s = 2\pi f (t_{p_{\max}} - t_{\Phi_{s,\max}}) \quad (34)$$

where $t_{\Phi_{tot,\max}}$, $t_{\Phi_{s,\max}}$ and $t_{p_{\max}}$ are the time corresponding to the peak of total heat-release-rate, the peak of heat-release-rate of species s and the pressure peak.

$p'_{\max}/\rho c^2$ is a solution input parameter, and has a fixed value when comparing chemical species. It is possible to correlate the fluctuations in the integrals of total heat-release-rate and the heat-release-rate of species s , as follows:

$$\frac{\Phi'_{tot}}{\bar{\Phi}_{tot}} = \sum_{s=1}^{N_s} \frac{\Phi'_s}{\bar{\Phi}_{tot}} \quad (35)$$

The sum of the species' heat-release-rate is equal to the total heat-release-rate. On the other hand, for studying the effects of each chemical species, it is necessary to consider the phase difference between the total heat-release-rate fluctuations and the species heat-release-rate fluctuations. As inferred from Fig. 2, in order to calculate the amount of heat-release-rate fluctuations by each species, it is necessary to multiply its corresponding amplitude by the cosine of the phase difference between the heat-release-rate of that species and total heat-release-

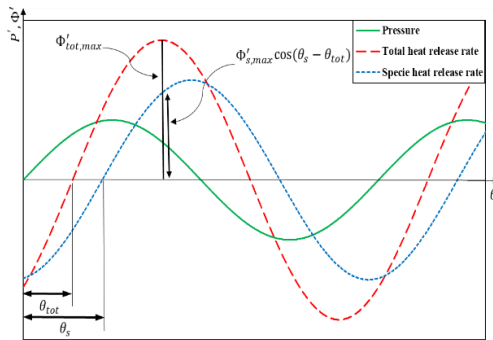


Fig. 2. Contribution of the heat-release-rate fluctuations for each species to the total heat-release-rate fluctuations (Phase difference included).

rate. By considering the amplitude of fluctuations and the phase difference simultaneously, the following equations are achieved:

$$\frac{\Phi'_{tot,\max}}{\bar{\Phi}_{tot}} = \sum_{s=1}^{N_s} \frac{\Phi'_{s,\max}}{\bar{\Phi}_{tot}} \cos(\theta_s - \theta_{tot}) \quad (36)$$

The above equations are used to study the effects of each chemical species.

2.6 Mesh Independence Study

The grid study was performed using five systematically refined meshes. The solution domain was divided into a reaction zone and a non-reaction

zone to achieve better accuracy and reduce the computational costs. Mesh size in the reaction zone is five times smaller than that in the non-reaction zone. Table 2 tabulates this information, including the number of computational points within the flame thickness in the reaction zone, and the number of total points in the solution domain.

The flame thickness can serve as a satisfying parameter when studying the independence of the solution from the mesh size. Figure 3 shows the calculated flame thickness corresponding to the five meshes of Table 2. Figure 4 also depicts the obtained heat-release-rate across the flame by these meshes. Based on the presented results, it is clear that the size of Mesh4 is adequate for capturing the steady flame without acoustic.

Furthermore, we have to show that the selected mesh size is suitable for simulating the interactions between acoustic waves and the flame. Figure 5 illustrates the time behavior of the non-dimensional

Table 2 Mesh study

Mesh	No. of point per flame thickness in reaction zone	No. of point in solution domain
Mesh 1	25	70
Mesh 2	50	140
Mesh 3	100	280
Mesh 4	200	560
Mesh 5	400	1120

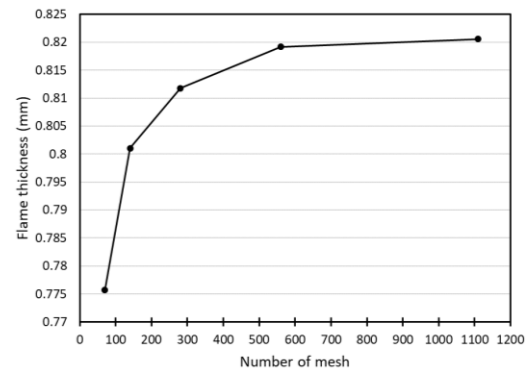


Fig. 3. Mesh independence for flame thickness.

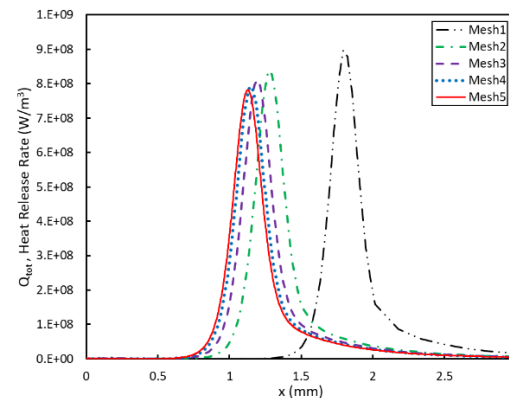


Fig. 4. Mesh independence for heat-release-rate across the flame without acoustic.

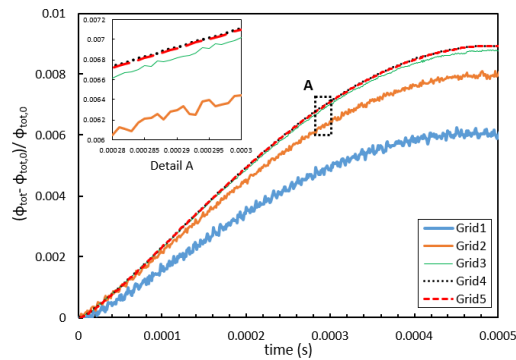


Fig. 5. Mesh independence for heat-release-rate fluctuations (flame with acoustic)

total heat-release-rate fluctuations for an interacting acoustic wave with a frequency of 500Hz is the total heat-release-rate of the steady flame without acoustic. The occurrence of some small spurious numerical oscillations on the results of coarser grids of Mesh1 and Mesh2 is noticeable. These numerical oscillations are emanated from the integration of the unresolved high gradients in the reaction zone. It is essential to prevent these unphysical oscillations for obtaining consistent results for the maximum non-dimensional value for fluctuations of the heat-release-rate integral, and its corresponding time. It is evident that adequately refining the grid can remove these wiggles from the results. Again, Mesh4 seems to be a suitable choice for this task.

Tuning the time step is also crucial for the present simulations. Due to a large number of chemical reactions with different time scales, the required time step needs to be very small. A suitable option would be in the order of 10^{-8} s. Larger values usually lead to divergence. However, smaller time steps of 5×10^{-9} s and 2.5×10^{-9} s were also examined, but almost identical results were obtained.

3. RESULTS

In this section, first the numerical results for the base flame model is presented, using various chemical mechanisms. As discussed before, the results of this section are used as the initial conditions for studying the interactions of acoustic waves and the flame in section 3.2. Furthermore, the effects of the acoustic waves on the total heat-release-rate fluctuations and chemical species are investigated, the data from various chemical mechanisms compared, and the effects of chemical species on the mechanisms discussed at the end.

3.1 Flame Without Acoustic

The base model is a laminar premixed flame in which the combustion of a Methane-Air mixture with an equivalence ratio of 0.625 in atmospheric pressure, the temperature of 300K, and velocity of 13cm/s occurs. The length of the computational domain is 7mm. Figure 6 compares the total heat-release-rate obtained from various chemical mechanisms. The results obtained from three GRI mechanisms are

compared in Fig. 6.a. It is observed that the calculated maximum heat-release-rate and the flame location by the GRI-1.2 and GRI-2.11 reaction mechanisms are close together, but they have a slight deviation from the results of the GRI-3.0 mechanism.

Figure 6.b compares the results of the GRI-1.2 mechanism and its reduced forms. The GRI-1.2 predicts the same maximum heat-release-rate for the different mechanisms and the only differences are in the flame location. Data for the 6-step mechanism with *drm19* and *drm22* show similarities, despite its much smaller number of chemical species and chemical reactions compared to the *drm19* and *drm22* mechanisms. Figure 6.c presents the calculated total heat-release-rate data for the GRI-2.11 mechanism and shows similarity in maximum heat-release-rate and a slight difference in the flame location. In this figure, it can also be seen that the results of the ARM2 and 12-step mechanisms are very similar. In Fig 6.d, GRI-3.0 and its reduced forms also predict similar heat-release-rate behavior, but again slight difference is seen in the flame location.

To conclude, Fig. 6 reveals that the prediction of the flame location by different chemical mechanisms differs slightly from each other. For explaining this difference, it is required to analyze the heat-release-rate for multiple chemical species. Figure 7.a shows the heat-release-rate of various chemical species across the solution domain. It is inferred that the maximum heat-release-rate of each species occurs at a different location across the flame. Total heat-release-rate can be calculated by adding up the amount of heat-release-rate from each chemical species. Hence, the amount of heat-release-rate from each chemical species contributes differently to the total heat-release-rate. It is observed in Fig. 7.a that H_2O has the most influential heat-release-rate, compared to the other chemical species. Therefore, H_2O is the primary contributor to the total heat-release-rate and the maximum location of the total heat-release-rate is mainly controlled by H_2O . Chemical reactions related to H_2O vary among different chemical mechanisms. Therefore, each mechanism provides different result for the location and value of maximum heat-release-rate of H_2O .

Also, to confirm this issue, the results of the GRI1.2, 6step and 10step mechanisms are compared in Figure 7.b. In this figure, for each mechanism, the amount of total and H_2O heat-release-rate is given. It can be seen that the location of maximum value of total heat-release-rate for each mechanism corresponds to its location of maximum H_2O heat-release-rate value.

Figure 8. shows variations in the mole fraction of chemical species predicted by the GRI-3.0 mechanism. Results for other mechanisms regarding these variations show a negligible difference. As mentioned before, the temperature, velocity, density, and molar fractions distributions calculated for the base flame model are used here as initial conditions for studying the effects of acoustic waves on the laminar flame in the following section.

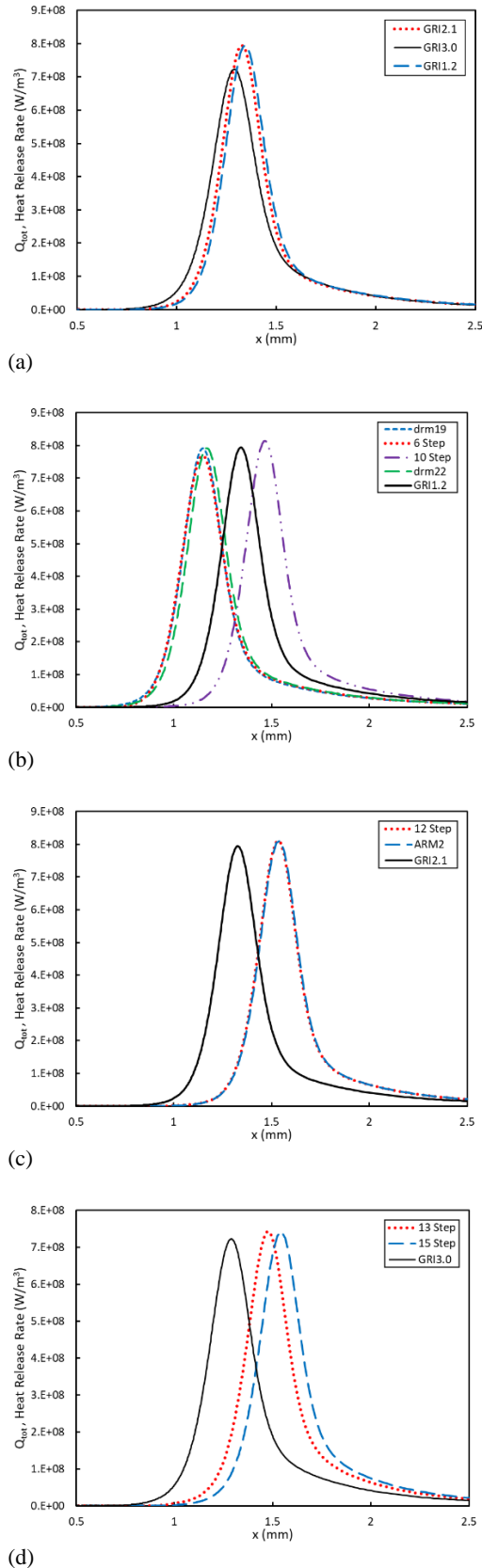


Fig. 6. Total heat-release-rate for flame without acoustic waves (a) GRI mechanism, (b) GRI-1.2 mechanism, (c) GRI-2.11 mechanism, (d) GRI-3.0 mechanisms).

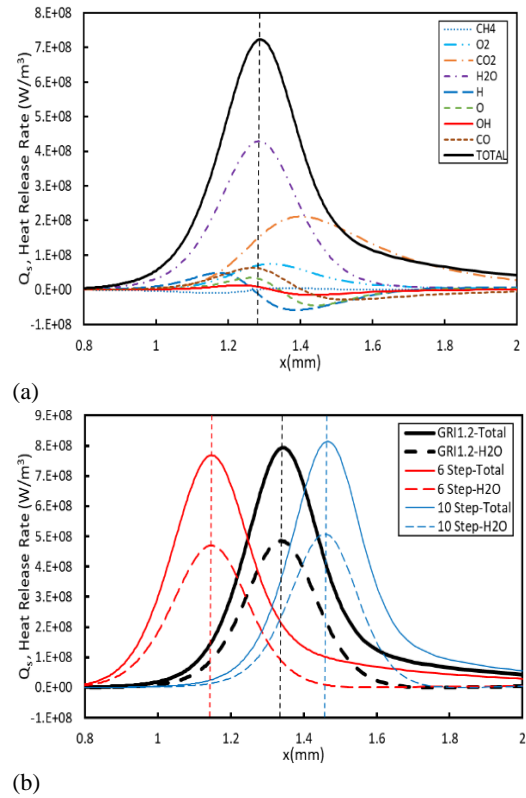


Fig. 7. (a) Heat-release-rate for various chemical species across the flame (flame without acoustic) (GRI-3.0) (b) Comparison of total and H₂O heat-release-rate for GRI1.2 and its reduced mechanisms.

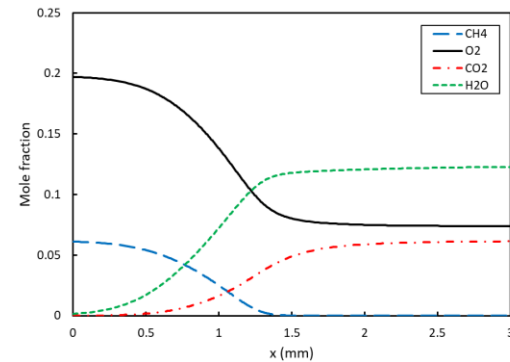


Fig. 8. Mole fractions of chemical species for flame without acoustic.

3.2 Flame-Acoustic Waves Interaction

3.2.1 Total Heat-Release-Rate Fluctuations

Considering different chemical reaction mechanisms, we assess the results for interaction between the flame and acoustic waves with an amplitude of 500 Pa (Jiménez *et al.* 2012) and a frequency in a range of 50-50000 Hz. Figure 9 compares the present numerical results for total heat-release-rate fluctuations at different frequencies, to the experimental data of (Wangher *et al.* 2008) and numerical data from (Jiménez *et al.* 2012).

Fluctuations for non-dimensional heat-release-rate fluctuations based on non-dimensional frequencies are presented in Fig. 9.a. It is evident that the predictions of the present study are in good agreement with data acquired by Jimenez *et al.* However, in spite of being in the same order of magnitude, there are discrepancies between numerical and experimental data. It is worth mentioning that no clear correlation is seen between the heat-release-rate fluctuations and frequency in the experimental data. The numerical results also show that the heat-release-rate fluctuations first increases by increasing the frequency in the range of 50-750Hz and then declines.

A phase difference is observed between the fluctuations in heat-release-rate and the acoustic wave at various frequencies. Based on Eq. 33, this phase difference is calculated and plotted in Fig. 9.b. The results show that by increasing frequency, a reduction in phase difference occurs. Moreover, there is a consistency between the numerical and

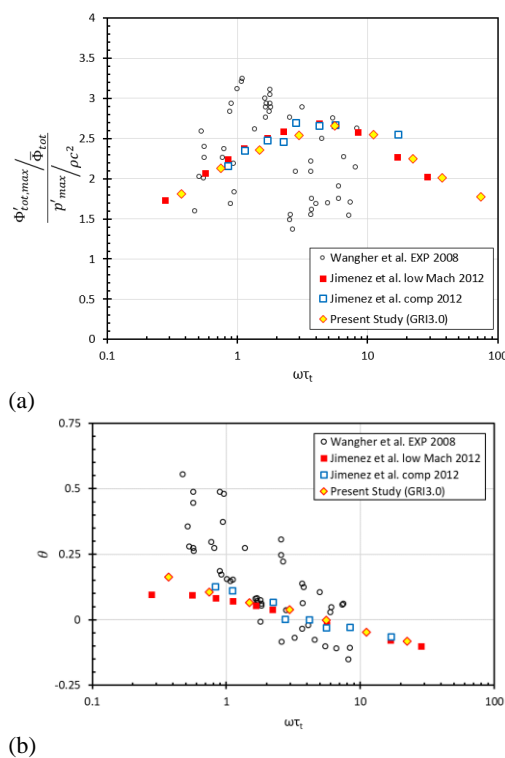


Fig. 9. (a) Total heat-release-rate fluctuations (b) Phase difference between acoustic waves and heat-release-rate fluctuations.

experimental data, but the regression line slope is larger for the experimental data. According to the Rayleigh’s instability criterion and the positivity of pressure fluctuations in the solution domain, one can infer that larger fluctuations in the heat-release-rate and smaller phase difference between pressure and heat-release-rate, results in more instability. Therefore, we can interpret the results of Fig. 9 as follow: because of smaller heat-release-rate fluctuations and higher phase differences at low frequencies, the system is more stable. The maximum expected instability occurs at 750Hz when

the heat-release-rate fluctuations are at the maximum level, and the phase difference is almost zero. Finally, more increase in the frequency results in less heat-release-rate fluctuations and more phase difference and ultimately leading to more stability.

3.2.2 Heat-release-rate Fluctuations of Chemical Species

The assessment of each chemical species contribution to the instability of a flame is critical. (Shalaby *et al.* 2009) studied the interaction between a turbulent premixed flame and acoustic waves and concluded that CO₂, H₂O, and H increase instability, and O, OH, and CO contribute to the dissipation of the acoustic waves. HCO, CH₂O, HO₂, and H₂O₂ radicals have little to no effect on the interaction process. It is understood that neutral species such as Argon (Ar) and Nitrogen (N₂), do not affect the process as well. (Laverdant and Thevenin 2003), studied the effects of Gaussian acoustic waves on a turbulent non-premixed Hydrogen flame and concluded that H₂O₂ and HO₂ have almost no effect, while H₂, O₂ and most importantly H₂O amplify the acoustic waves, and that H* is the primary contributor to the dissipation of the acoustic waves.

(Beardsell and Blanquart, 2019) calculated the interactions of acoustic waves with a laminar premixed Methane-Air flame. By plotting the maximum amounts for chemical species mass fractions, they studied the effects of each species. They reached the conclusion that if maximum mass fractions for O* and H* are in the same phase as the total heat-release-rate fluctuations and the acoustic waves, total heat-release-rate fluctuations will be at maximum. However, they did not study the effects of other chemical species.

In this study and according to Rayleigh’s instability criterion, the effects of other species is assessed using Eq. (36). The amount of θ for the primary contributors is presented in Fig. 10.a. Other chemical species have little to no effect, and are disregarded. It is understood that H₂O and CO₂ have a similar behavior regarding the contribution to the total heat-release-rate fluctuations. However, O*, H*, and OH* have a low amplitude of the heat-release-rate fluctuations at low frequencies, and with the increase of frequency, their amplitude rises, where at higher frequencies, their amplitude is higher than H₂O and CO₂. To study the effects of each chemical species, it is necessary to consider phase difference (Fig. 2). The phase difference of each chemical species with total heat-release-rate fluctuations is presented in Fig. 10.b. The gradient of phase difference in O* and H* is noticeably larger than H₂O and CO₂.

Using Eq. (36), the impact of each species on the total heat-release-rate fluctuations is plotted in Fig. 10.c, as well as the effect of the instability of each species according to its sign and magnitude. Negative values refer to species that contribute to stability, while positive values refer to species that contribute to instability. In Fig. 10.b, stability and instability contributions for each chemical species can be calculated based on their phase difference. -

$\pi/2$ to $\pi/2$ is the range for instability, while $-3\pi/2$ to $-5\pi/2$ is the range for stability.

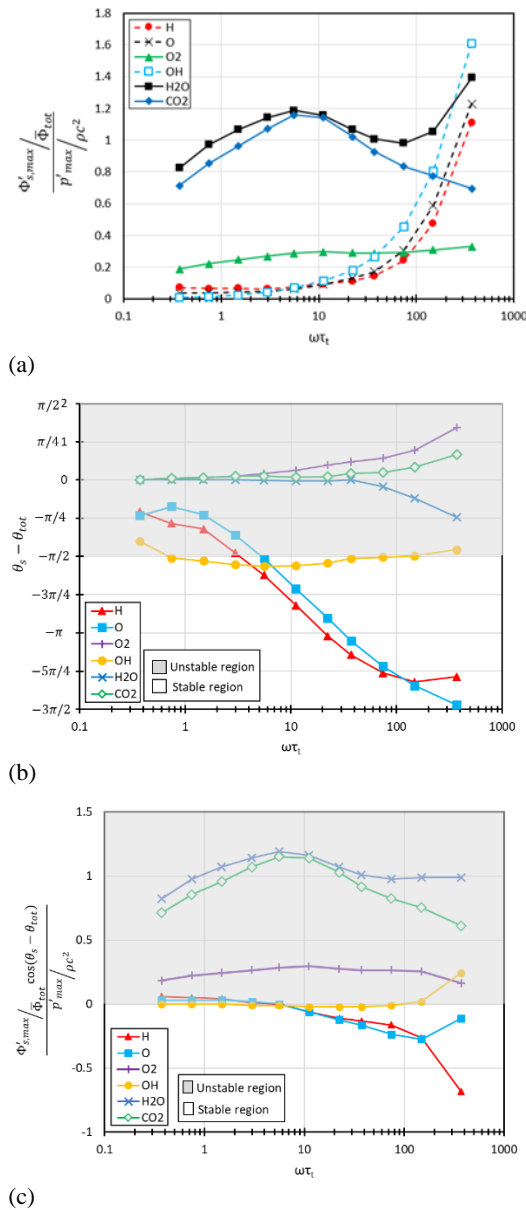


Fig. 10. (a) Heat-release-rate fluctuations for different chemical species, (b) Phase difference between acoustic waves and heat-release-rate fluctuations of chemical species, (c) Heat-release-rate fluctuations for each chemical species based on phase difference.

According to Fig. 10.b and 10.c, chemical species can act as both stabilizers and destabilizers at different frequencies. At low frequencies, O and H have destabilizing effects in the $-\pi/2$ to $\pi/2$ range. Although, because of insignificant amplitude of fluctuations, this has very little effect. At higher frequencies, they have stabilizing effects and because of significant amplitude of fluctuations, they contribute majorly to stability. H₂O and CO₂ have a large amplitude of fluctuations and phase difference

in the instability range, and act as destabilizing factors. At high frequencies, OH has a large amplitude of fluctuations, but because of having a phase difference near $-\pi/2$, it has little to no effect on total heat-release-rate fluctuations and stability.

3.2.3 Comparison of Different Mechanisms

The various chemical kinetic mechanisms can be used in numerical simulation of combustion. The selection of each mechanism is based on the degree of accuracy and cost-effectiveness. The computational cost would considerably increase as more chemical species are taken into account. The number of chemical species equations is equal to the number of species selected for the chemical kinetic mechanism. In order to calculate the interactions between the flame and acoustic waves in industrial applications, it is necessary to use the LES model. Unsteady and three-dimensional solutions, along with multi-step chemical kinetic mechanisms, are costly and time consuming. Therefore, most of the researchers generally use single-step mechanisms.

(Schmidt and Jiménez 2010) numerically simulated the interaction between the flame and acoustic waves using three single-step mechanisms, GRI-3.0, and the Peter's model. They concluded that in order to simulate the interaction properly, it is necessary to use multi-step mechanisms. Peter's model and GRI-3.0 are mechanisms with multiple species and reactions, but are computationally expensive. In this section, the behavior of the GRI mechanism and its reduced forms in studying interaction of flame and acoustic waves are explored. The difference between the data acquired from these mechanisms is due to the influences of several contributing species.

Figure 11 shows the obtained results by these GRI mechanisms for the non-dimensional fluctuations of the total heat-release-rate in terms of the non-dimensional acoustic wave frequency. The frequency at which the total heat-release-rate fluctuations reaches to the maximum value is similar in all of the mechanisms. On the other hand, as Fig. 11.a shows, the 13-step reduced form of GRI-3.0 is in better agreement with its original mechanism than the 15-step mechanism. This indicates that considering more steps does not guarantee accuracy. However, data obtained from GRI-2.11 and its reduced forms in Fig. 11.b show that the 12 and 16-step ARM2 reduced forms of GRI-2.11 produce similar results but are not in good agreement with the data acquired by GRI-2.11. These mechanisms show the most difference with their original form. In Fig. 11.c, data from GRI-1.2 and its reduced forms are presented. Since the dr22 and dr19 (reduced forms of GRI-1.2) results are the same again, only results of dr19 are presented. The 6-step mechanism also produced similar data to dr19, with a little difference at higher frequencies. The 10-step mechanism shows similarities with data from GRI-1.2 at lower frequencies.

Based on similar data obtained from the reduced forms of the GRI mechanisms, it is concluded that the less costly reduced forms are superior for the calculation purpose. The 6 and 10-step mechanisms

show the most similar data to those acquired from the GRI mechanisms. These two mechanisms involve fewer species, compared to the GRI mechanisms, and need less transport equations.

The difference in data obtained from these mechanisms comes from the different chemical

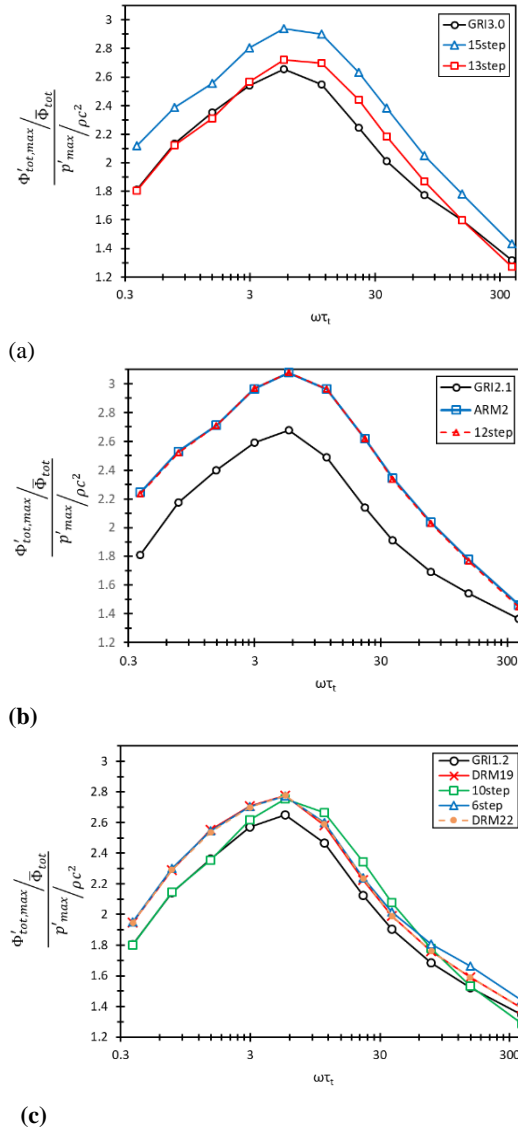


Fig. 11. Amplitude of fluctuations for total heat-release-rate ((a) GRI-3.0 and its reduced forms, (b) GRI-2.11 and its reduced forms, (c) GRI-1.2 and its reduced forms).

reactions selected for each mechanism. Similarities between the 12- and 16-step (ARM2) mechanisms are because they share 10 almost identical chemical reactions. In order to investigate the difference between these mechanisms, the heat-release-rate fluctuations from each species must be evaluated.

Data obtained from the 12-step mechanism has the most differences to the data from the GRI mechanisms. To analyze this difference, the 12-step

mechanism is compared to the 13-step mechanism. The 13-step mechanism has 14 species, 13 of which are identical to the 12-step mechanism. Only NH_3 , which is a minor chemical species, is added to the 13-step mechanism. These two mechanisms have 4 almost identical chemical reactions. The amplitude of fluctuations for the non-dimensional heat-release-rate in the 12 and 13-step mechanisms is presented in Fig. 12. It is implied that the behavior of heat-release-rate fluctuations in both mechanisms is similar. Nonetheless, the difference in heat-release-rate fluctuations of H_2O is significant. The 13-step mechanism's superiority is due to a better prediction of H_2O . Chemical reaction related to H_2O for the 12-step mechanism is presented in Eq. (37), and that of the 13-step mechanism is presented in Eqs. (38) and (39). H_2O is obtained via a single chemical reaction in the 12-step mechanism, while in the 13-step mechanism; this has been achieved via two chemical reactions. Such simplification in the 12-step mechanism is the reason that it predicts the behavior of H_2O poorly compared to the 13-step mechanism.

The 6-step mechanism is the most cost-efficient selection, which also has good accuracy. The other

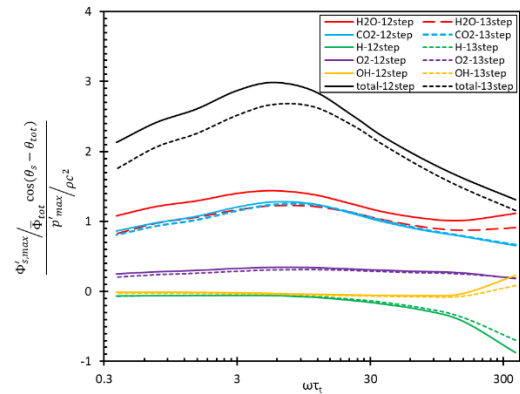
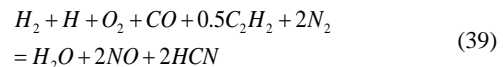
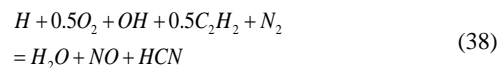


Fig. 12. Amplitude of fluctuations for heat-release-rate of each chemical species (from the 12 and 13-step mechanisms).

advantage it has compared to other accurate mechanisms (10step and 13step mechanisms) is the inclusion of O and its corresponding chemical reactions. In Fig. 13, fluctuations for heat-release-rate of each chemical species for GRI-3.0 and the 6-step mechanism have been presented. It is understood that the 6-step mechanism produces data very similar to GRI-3.0, the only difference is in the behavior of H_2O .

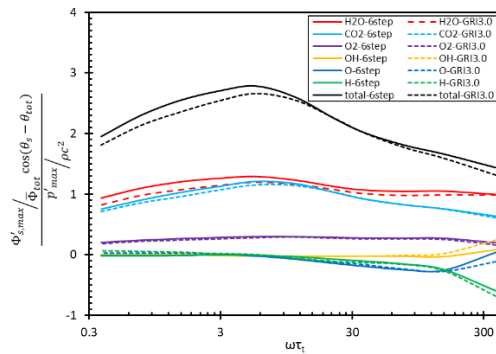


Fig. 13. Amplitude of fluctuations for heat-release-rate of each chemical species (from GRI-3.0 and the 6-step mechanism).

5. CONCLUSION

In this study, interaction between a one-dimensional Methane-Air laminar premixed flame and acoustic waves with a frequency of 50-50000Hz have been simulated. Equations for chemical species transport, energy, state and velocity were solved in one space dimension. Data acquired from this study was in good agreement with experimental and numerical data from other researches. Any change in the frequency of the acoustic waves affects fluctuations of heat-release-rate. Phase difference between fluctuations of heat-release-rate and pressure decreases when the frequency is increased. By assessing each chemical species heat-release-rate fluctuations, their effect on total heat-release-rate fluctuations and instability were determined. H₂O, CO₂ and O₂ have the most impact on total heat-release-rate fluctuations, respectively. These species have a destabilizing effect. H*, O* and OH* also have a significant impact on total heat-release-rate fluctuations. H* and O* have a destabilizing effect at low frequencies, but have a stabilizing effect at higher frequencies.

GRI mechanisms and their reduced forms were assessed in order to obtain an accurate and cost-efficient mechanism. All of the reduced form mechanisms predicted the frequency related change in heat-release-rate fluctuations correctly. Difference in predicting the behavior of H₂O is understood to be the source of difference in data obtained from these mechanisms. The 6-step mechanism is a cost-efficient and accurate mechanism; it also has few chemical species and reactions. Therefore, it is determined to be well-suited for this line of study.

REFERENCES

Baum, M., T. Poinso and D. Thévenin (1995). Accurate boundary conditions for multicomponent reactive flows. *Journal of Computational Physics* 116(2), 247–261.

Beardsell, G. and G. Blanquart (2019). Impact of pressure fluctuations on the dynamics of laminar premixed flames. *Proceedings of the Combustion Institute* 37(2), 1895–1902.

Beardsell, G. and G. Blanquart (2021). Fully compressible simulations of the impact of acoustic waves on the dynamics of laminar premixed flames for engine-relevant conditions. *Proceedings of the Combustion Institute* 38(2), 1923–1931.

Bowman, C. T., R. K. Hanson, D. F. Davidson, W. C. Gardiner, V. Lissianski, G. P. Smith D. M. Golden, M. Frenklach and M. Goldenberg (n.d.). *GRI-Mech* 2.11.

Chang, W. C. and J. Y. Chen (n.d.). Reduced Mechanisms based on GRI-Mech 1.2. [Http://Firebrand.Me.Berkeley.Edu/GriREDU.Html](http://Firebrand.Me.Berkeley.Edu/GriREDU.Html).

Chao, Y. C., T. Yuan and C. S. Tseng (1996). Effects of flame lifting and acoustic excitation on the reduction of NO_x emissions. *Combustion Science and Technology* 113–114, 49–65.

Chen, J. Y. (n.d.). Reduced Mechanisms based on GRI-Mech. <https://tnfworkshop.org/chemistry/>

Clavin, P. A. U. L. and P. Pelce (1989). *One-Dimensional Vibratory Instability of Planar Flames Propagating in Tubes*. Published online by Cambridge University Press.

Clavin, P. and G. Searby (2008). Unsteady response of chain-branching premixed-flames to pressure waves. *Combustion Theory and Modelling* 12(3), 545–567.

Demare, D. and F. Baillet (2004). Acoustic enhancement of combustion in lifted nonpremixed jet flames. *Combustion and Flame* 139(4), 312–328.

Fernandez-Tarrazo, E., A. L. Sánchez, A. Linan and F. A. Williams (2006). A simple one-step chemistry model for partially premixed hydrocarbon combustion. *Combustion and Flame* 147(1–2), 32–38.

Frenklach, M., H. Wang, M. Goldenberg, G. P. Smith, D. M. Golden, C. T. Bowman, R. K. Hanson, W. C. Gardiner and V. Lissianski (1995). Gri-mech: An optimized detailed chemical reaction mechanism for methane combustion. In *Topical Report*, SRI International, Menlo Park, CA (United States).

Fujisawa, N., K. Iwasaki, K. Fujisawa and T. Yamagata (2019). Flow visualization study of a diffusion flame under acoustic excitation. *Fuel* 251, 506–513.

Hajjaligol, N. and K. Mazaheri (2017). Thermal response of a turbulent premixed flame to the imposed inlet oscillating velocity. *Energy* 118, 209–220.

Han, X. and A. S. Morgans (2015). Simulation of the flame describing function of a turbulent premixed flame using an open-source LES solver. *Combustion and Flame* 162(5), 1778–1792.

- Han, X., J. Yang and J. Mao (2016). LES investigation of two frequency effects on acoustically forced premixed flame. *Fuel* 185, 449–459.
- Jiménez, C., J. Quinard, J. Graña-Otero, H. Schmidt, and G. Searby (2012). Unsteady response of hydrogen and methane flames to pressure waves. *Combustion and Flame* 159(5), 1894–1908.
- Kazakov, A. and F. Frenklach (n.d. a). *DRM19*. <http://combustion.berkeley.edu/drm/>
- Kazakov, A. and F. Frenklach (n.d. b). *DRM22*. <http://combustion.berkeley.edu/drm/>
- Kee, R. J., F. M. Rupley and J. A. Miller (1989). *Chemkin-II: A Fortran Chemical Kinetics Package for the Analysis of Gas-Phase Chemical Kinetics*. SAND89-8009, Sandia National Laboratories.
- Klein, R. (1995). Semi-Implicit Extension of a Godunov- Type Scheme Based on Low Mach Number Asymptotics 1:One-Dimensional Flow. *Journal of Computational Physics* 121, 213–237.
- Laverdant, A. and D. Thevenin (2003). Interaction of a Gaussian acoustic wave with a turbulent premixed flam. *Combustion and Flame* 134, 11–19.
- Lee, C. Y. and S. Cant (2017). LES of Nonlinear Saturation in Forced Turbulent Premixed Flames. *Flow, Turbulence and Combustion* 99(2), 461–486.
- Massey, J. C., I. Langella and N. Swaminathan (2018). Large Eddy Simulation of a Bluff Body Stabilised Premixed Flame Using Flamelets. *Flow, Turbulence and Combustion* 101(4), 973–992.
- Mcintosh, A. C. (1991). Pressure disturbances of different length scales interacting with conventional flames. *Combustion Science and Technology* 75(4–6), 287–309.
- Mcintosh, A. C. (1993). The linearised response of the mass burning rate of a premixed flame to rapid pressure changes. *Combustion Science and Technology* 91(4–6), 329–346.
- Mcintosh, A. C. (1999). Deflagration fronts and compressibility. *Philosophical Transactions of the Royal Society of London A: Mathematical, Physical and Engineering Sciences* 357(1764), 3523–3538.
- Oh, J., P. Heo and Y. Yoon (2009). Acoustic excitation effect on NO_x reduction and flame stability in a lifted non-premixed turbulent hydrogen jet with coaxial air. *International Journal of Hydrogen Energy* 34(18), 7851–7861.
- Peters, N. (1996). Fifteen lectures on laminar and turbulent combustion. *Ercoftac Summer School* 1428, 245.
- Rayleigh, J. S. W. (1945). *Theory of Sound*. Dover Publications; Unabridged Second Revised Edition.
- Saxena, P. and F. A. Williams (2006). Testing a small detailed chemical-kinetic mechanism for the combustion of hydrogen and carbon monoxide. *Combustion and Flame* 145(1–2), 316–323.
- Schmidt, H. and C. Jiménez (2010). Numerical study of the direct pressure effect of acoustic waves in planar premixed flames. *Combustion and Flame* 157(8), 1610–1619.
- Shalaby, H., A. Laverdant and D. Thévenin (2009). Direct numerical simulation of a realistic acoustic wave interacting with a premixed flame. *Proceedings of the Combustion Institute* 32 I, 1473–1480.
- Shreekrishna, S. and T. Liewwen (2009). High frequency premixed flame response to acoustic perturbations. In *15th AIAA/CEAS Aeroacoustics Conference (30th AIAA Aeroacoustics Conference)*.
- Smith, G. P., D. M. Golden, F. Frenklach, N. W. Moriarty, B. Eiteneer, M. Goldenberg, C. T. Bowman, R. K. Hanson, S. Song, W. C. Gardiner, V. V. Lissianski and Z. Qin (n.d.). *GRI-Mech* 3.0. http://www.me.berkeley.edu/gri_mech/
- Sung, C. J., C. K. Law and J. Y. Chen (2001). Augmented reduced mechanisms for NO emission in methane oxidation. *Combustion and Flame* 125(1–2), 906–919.
- Liewwen, T. C. and V. Yang (2005). *Combustion Instabilities in Gas Turbine Engines: Operational Experience, Fundamental Mechanisms, and Modeling*. American Institute of Aeronautics and Astronautics.
- Tang, Q. (2003). *Ph. D. Thesis. Computational Modelling of Turbulent Combustion with Detailed Chemistry*. Cornell University.
- Wangher, A., G. Searby and J. Quinard (2008). Experimental investigation of the unsteady response of premixed flame fronts to acoustic pressure waves. *Combustion and Flame* 154(1–2), 310–318.